

Measurements of convective and radiative heating in wildland fires

David Frankman^A, Brent W. Webb^A, Bret W. Butler^{B,E}, Daniel Jimenez^B, Jason M. Forthofer^B, Paul Sopko^B, Kyle S. Shannon^B, J. Kevin Hiers^C and Roger D. Ottmar^D

^ADepartment of Mechanical Engineering, Brigham Young University, Provo, UT 84602, USA.

^BUS Forest Service, Rocky Mountain Research Station, Fire Sciences Laboratory, 5775 Highway 10 W, Missoula, MT 59808, USA.

^CEglin Air Force Base, Jackson Guard, 107 Highway 85 N, Niceville, FL 32578, USA.

^DUS Forest Service, Pacific Northwest Research Station, 400 N 34th Street, Suite 201, Seattle, WA 98103, USA.

^ECorresponding author. Email: bwbutler@fs.fed.us

Abstract. Time-resolved irradiance and convective heating and cooling of fast-response thermopile sensors were measured in 13 natural and prescribed wildland fires under a variety of fuel and ambient conditions. It was shown that a sensor exposed to the fire environment was subject to rapid fluctuations of convective transfer whereas irradiance measured by a windowed sensor was much less variable in time, increasing nearly monotonically with the approach of the flame front and largely declining with its passage. Irradiance beneath two crown fires peaked at 200 and 300 kW m⁻², peak irradiance associated with fires in surface fuels reached 100 kW m⁻² and the peak for three instances of burning in shrub fuels was 132 kW m⁻². The fire radiative energy accounted for 79% of the variance in fuel consumption. Convective heating at the sensor surface varied from 15% to values exceeding the radiative flux. Detailed measurements of convective and radiative heating rates in wildland fires are presented. Results indicate that the relative contribution of each to total energy release is dependent on fuel and environment.

Received 12 July 2011, accepted 27 June 2012, published online 11 September 2012

Introduction

Radiative and convective heat transfer play complementary roles in wildland fire spread (Anderson 1969; Yedinak *et al.* 2006; Anderson *et al.* 2010). In order to understand and accurately predict the behaviour of wildland fires (Albini 1996), to model fire emissions and energy release (Wooster *et al.* 2005; Freeborn *et al.* 2008) and to improve public and wildland firefighter safety (Butler and Cohen 1998) it is necessary to understand how energy is released from wildland fires. Although several studies have reported measurements of energy transport from biomass-fuelled flames, their scope is limited and has primarily been radiative energy transport. Improved understanding of how energy is transported through both radiative and convective modes in wildland fires remains a critical yet poorly documented element of wildland fire science.

Packham and Pompe (1971) reported radiative heat flux in a slash fire in Australian forest lands. The flame irradiance was measured using a vertical King radiometer (King 1961). Heating reached 100 kW m⁻² when the flame was adjacent to the sensor and 57 kW m⁻² when the sensor was a distance 7.6 m from the flame. Butler *et al.* (2004) presented temporally and spatially resolved irradiance measurements in a boreal forest crown fire.

The vegetation was primarily jack pine (*Pinus banksiana*) with an understory of black spruce (*Picea mariana*). A thermopile-based sensor (Butler 1993) with a response time of 0.05 s measured the heat flux at a sample rate of 1 Hz. Irradiance values averaged 200 kW m⁻² with a maximum value of 290 kW m⁻² in the flame. Morandini *et al.* (2006) measured time-resolved irradiance values 5, 10 and 15 m from flames burning in 2.5 m-tall Mediterranean shrubs (*Olea europea*, *Quercus ilex*, *arbustus unedo*, *Cistus Monspeliensis* and *Cytisus triflorus*). Both total and radiative heat fluxes incident on the sensor face were measured but the sensors were not close enough to the flames to experience any convection. The radiative heat flux incident on the sensor (irradiance) was measured using Captec sensors (Captec Enterprise, Lille, France) (Santoni *et al.* 2006), which have a 50-ms response time. Sensors were sampled at 100 Hz. Radiative heat fluxes ranged between 7 and 8 kW m⁻². Silvani and Morandini (2009) measured time-resolved radiative and total heat fluxes incident on the sensor in four experiments burning pine needles and oak branches. These data were sampled using Medtherm 64 sensors (Medtherm Corporation, Huntsville, AL) at 1 Hz. The response time of these sensors was nominally 250 ms at heat flux levels

below 341 kW m^{-2} . Peak radiative and total heating at the sensor were 50 and 110 kW m^{-2} . Others report a series of experiments designed to characterise the vertical distribution of exitance from wildland flames (Cruz *et al.* 2011). Peak radiant fluxes reached 176 kW m^{-2} with a clear dependence on height within the flames.

The extreme environment of wildland fires limits measurement methods. Nevertheless, the reported studies have increased understanding of the magnitudes of radiative and total energy release from wildland flames although there is still much that is not understood, particularly with regard to the temporal and spatial characteristics of convective heat transfer in wildland fires. The reported works suggest that sensor type, deployment orientation and location relative to the fire front can significantly influence the measurements, thus complicating comparison of results. Here we report time-resolved convective and radiative heat fluxes, produced by fires burning in a variety of vegetation and terrain types, and seek to correlate and generalise the measurements with respect to the fire, fuel and environmental conditions. It is intended that these measurements inform new understanding about the relative contribution of radiative and convective heating to overall energy transport in and around wildland fires under a variety of conditions.

Measurement procedure

A sensor configuration consisting of two HFM-7 heat flux microsensors manufactured by Vatel Corp. was constructed (Christiansburg, VA). The sensors consist of a differential thermopile heat flux gauge formed by a $2 \text{ }\mu\text{m}$ -thick layer of three materials deposited on a substrate mounted on the end of a 6-mm diameter by 12.7 mm-long copper cylinder. Each sensor was coated with a highly absorbent paint ($\epsilon = 0.94$), has a $300\text{-}\mu\text{s}$ response time and includes a platinum resistance temperature sensor (<http://www.vatell.com/hfm.htm>, accessed 18 October 2011). For this study two of the copper cylinders containing the heat flux gauge and temperature sensor were mounted in a rectangular aluminium housing (0.05 by 0.05-m square cross-section as shown in Fig. 1) designed to act as a heat sink. The aluminium sensor housing was insulated with a 1 to 2 cm-thick layer of ceramic wool and covered with reflective aluminium foil. As heat

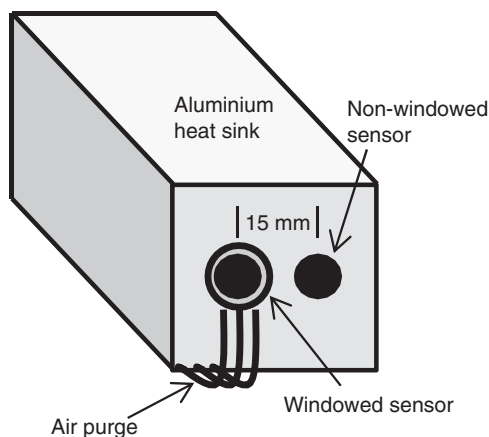


Fig. 1. Diagram of sensor setup.

flows into or out of the thermopile substrate a small temperature difference is produced. The sensor operates by measuring the rate of thermal energy flow per unit area (heat flux) and the temperature at its front surface simultaneously. The polarity of the signal indicates direction of heat flow and the magnitude is proportional to heat flux. A 0.5 mm-thick sapphire window was mounted over one of the two sensors, whereas the other sensor was left exposed. The field of view of the sensors was a cone of rotation prescribed by a 160° subtended angle. The sensor and window mounts were designed so that both sensors had the same field of view, and both sensors were mounted with the active surfaces oriented vertically so as to detect incident heat transfer nominally in the incoming horizontal direction. The windowed sensor had a 0.5-mm air gap between the sensor face and the internal window surface and the external surface of the window was continuously purged with air to prevent fouling by soot or other combustion byproducts. Tests were conducted to confirm that the purge air flow rate kept the window clean but did not affect the adjacent non-windowed sensor signal. The non-windowed sensor gathered total (convective plus radiative) heat transfer whereas the windowed sensor gathered only radiative energy (after some quantified and corrected loss in transmission through the window). Voltages from the sensors were simultaneously sampled at a user specified rate that varied between 5 and 100 Hz, well within the frequency response of the sensors. In all cases the sensors were located ~ 0.5 m above ground level.

Flame front rate of spread, flame length, flame angle from the vertical, flame depth and flaming combustion residence time were computed from visual-based analysis of in-fire video records. In most cases the measurements represent the average of three or more observations.

For the purposes of this discussion, convective and radiative heat flux are defined as a flow of energy per unit time through a unit area and units are W m^{-2} . Irradiance is the radiative energy flux arriving at the surface per unit area and exitance is the emitted energy per unit area (typically referring to energy emitted from the flames). At an arbitrary location in front of an advancing flame the irradiance depends on such factors as flame shape, combustion steadiness, distance between the flame and the sensor, among others. By contrast, in theory the exitance from an advancing flame should be constant as long as the flame is burning under relatively constant fuel and environmental conditions. Thus, the measurements presented here represent irradiance, except when the flames engulf the sensor at which time the sensed values may be interpreted to be exitance of the flame for the volume of flame within the sensor field of view. In any case the sensors sample energy from a nearly hemispherical field of view including the atmosphere and ground in front of, above and below the sensors. Thus, the sensed energy represents a directional integration of the total energy emitted from all sources within the field of view. The convective calculation is for the face of the sensor only and does not include any spatial averaging as is the case for the radiative energy values.

The sensors were calibrated by the manufacturer in a blackbody cavity environment, such that the radiative flux incident on the sensor (or irradiance) was known as a function of the controlled blackbody cavity temperature. The calibration thus yielded the incident radiative flux ($q''_{rad,inc}$) for the sensor in a

radiation-only environment where diffuse black body behaviour was imposed:

$$q''_{cal} = q''_{rad,inc} \quad (1)$$

Practically speaking, each sensor responded only to energy passing through the thermopile, irrespective of the form (radiative or convective) in which the energy was delivered. Thus, only heat flux absorbed by the sensor (q''_{abs}) resulted in a voltage response, and the absorbed radiation heat was a fraction of the incident heat flux on the sensor surface, the scaling factor being the emissivity of the sensor surface (ε):

$$q''_{abs} = \varepsilon q''_{rad,inc} \quad (2)$$

Eqns 1 and 2 are general expressions for sensors exposed to convective and radiative modes of heat transfer acting in a combined fashion or independently. The absorbed flux that results in sensor response voltage is related to either the convective, radiative or combined flux. The heat flux absorbed by the windowed sensor ($q''_{abs,w}$) is equal to the radiative heat flux incident on the outside of the window ($q''_{rad,inc}$) scaled by the emissivity of the sensor surface and the effective window transmittance (τ):

$$q''_{abs,w} = \tau \varepsilon q''_{rad,inc} \quad (3)$$

The effective transmittance of the sapphire window was experimentally measured by igniting 400 g of aspen (*Populus tremuloides*) wood shavings 1 m from the two sensors. This distance was selected to ensure that no hot buoyancy-driven flow from the flame would come into contact with the sensors. Thus, both sensors (non-windowed and windowed) were exposed to the same radiative heating-only environment. Time-resolved voltage data were collected for both windowed and non-windowed sensors in this configuration, the incident flux based on the factory calibrations were determined for both sensors ($q''_{cal,w}$ and $q''_{cal,nw}$) and the effective transmittance τ of the window when exposed to thermal radiation from a flame burning woody fuels (similar to what would be encountered in field measurements) was determined by calculating the time-average of the ratio of the two magnitudes:

$$\tau = \text{average} \left(\frac{q''_{cal,w}}{q''_{cal,nw}} \right) \quad (4)$$

Using this method, the value of τ was determined to be 0.62. This value was derived from the mean of over 2000 measurements collected over 40 s during the period of peak flaming. A student's *t*-confidence interval indicates 90% probability that the true mean is between 0.57 and 0.67.

Substituting Eqn 2 into Eqn 3, and solving for the radiation incident on the outside of the sapphire window yields:

$$q''_{rad,inc} = q''_{cal,w}/\tau \quad (5)$$

The heat flux absorbed by the non-windowed sensor is the sum of the incident radiative flux that is absorbed and the convective flux:

$$q''_{abs,nw} = \varepsilon q''_{rad,inc} + q''_{conv} \quad (6)$$

where q''_{conv} is the convective heat flux. Substituting Eqn 2 and 5 into Eqn 6 yields:

$$\varepsilon q''_{cal,nw} = (\varepsilon q''_{cal,w}/\tau) + q''_{conv} \quad (7)$$

Solving Eqn 7 for the convective heat flux yields:

$$q''_{conv} = \varepsilon(q''_{cal,nw} - q''_{cal,w}/\tau) \quad (8)$$

Assuming that the spectra of the calibration flame and the wildland fire flame are similar, the temporal characteristics of the fluctuating incident radiative and convective flux were respectively calculated from Eqn 5 and Eqn 8. Convective heat flux values calculated in Eqn 8 are a strong function of the geometry of the sensor housing, the local flow field, and the surface temperature and properties. Thus it is difficult to interpret these measurements within the context of small diameter or thickness vegetation elements. Given the diversity of shapes, sizes and thermal properties of grasses, leaves, stems and needles it would be impossible to design sensors that exactly represent the convective heating of vegetation elements. However, data collected using the sensors and process outlined here can provide information regarding the partitioning of convective and radiative flux in front of and during flame exposure in a wildland fire environment and the temporal properties of convective heating that vegetation elements would be exposed to in and around flames.

The measurement uncertainty associated with the sensor setup was characterised by sampling 500 points before the arrival of the fire (essentially defining the sensor zero level signal). The uncertainty magnitude associated with this test was estimated to be $\pm 0.17 \text{ kW m}^{-2}$ for radiation and $\pm 0.13 \text{ kW m}^{-2}$ for convection with 99% confidence. Measurement bias was minimised by adjusting the voltage output of the sensors at thermal equilibrium after amplification to a mean of zero. A second source of measurement uncertainty is associated with heating of the sensors. The temperature rise of the sensors was no more than 30°C above ambient for all the field burns. A maximum sensor temperature of 58°C gives rise to an error of less than 0.68 kW m^{-2} in the radiative flux suggesting that the thermal mass of the housing and the insulation was sufficient to prevent significant measurement uncertainty.

The sensors were oriented to face the most likely direction of flame approach. The direction of flame spread was towards the sensors in roughly three-quarters of the deployments. The flame spread laterally across the sensors for the remainder of the deployments.

In all cases the sensors measured the radiant and convective energy arriving at the sensor face. However, the peak values were collected when the sensor was engulfed in flames, and the peak values may therefore be interpreted as flame energy emitted by the flames either by radiative or convective energy

transport for a variety of fuel, terrain and environmental conditions. Table 1 summarises the conditions and location of each dataset. Table 2 summarises the measured variables for each dataset.

Results

The data are represented in three groups: those that burned primarily in surface fuels, those that included a significant brush component and those that burned as crown fires. The instrument locations are depicted in the photographs of Fig. 2a–j, and subsequent figures present the measurements.

Surface fires

The first dataset was collected on the Rombo Mountain Fire on 28 August 2007 (designated Rombo 1). Table 1 presents site and environment details. Fig. 2a shows the instrument site where the fuels consisted primarily of mixed grasses and ponderosa pine (*Pinus ponderosa*) needle cast. Fuel consumed in the flaming combustion was estimated from the digital photo series PPJ 07 (Ottmar et al. 2007) to be 0.47 kg m⁻². The convective heat flux rises dramatically between 150 and 200 s into the burn (Fig. 3a). The radiative flux has a peak of 20 kW m⁻². The convective flux fluctuates dramatically between -5 and 22 kW m⁻². Negative values (or cooling) can be explained by the presence of packets of cool air sweeping past the sensor after the sensor has been slightly heated by positive radiative or convective heat flux. Flame rate of spread and geometry are presented in Table 2.

When viewing the lower panel in Fig. 3a, the fluctuations in the convective flux obscure the ability to determine whether the sensor is primarily being heated or cooled. To clarify this point a running fraction was computed and is shown in the upper panel of Fig. 3a. The data in the upper panel characterise the rapid fluctuations seen in the convective heat flux by a running fraction of time since convective heating or cooling began. A data point is considered to show heating if the value is above 1 kW m⁻² and cooling if it is below -1 kW m⁻². The definition of the commencement of the convective event is somewhat arbitrary; however, the fraction heating and cooling parameters thus defined are meant to provide a quantitative measure of the time the sensors spend under heating and cooling conditions. The convective heating and cooling fractions illustrated in Fig. 3a rise from a zero value (indicated by a heat flux near zero (i.e. between -1 and 1 kW m⁻²) at the time origin arbitrarily selected for this dataset), peak within the first 100 s of the event and represent at most ~25% of the total energy arriving at the sensor. Subsequently they decline as the intensity of the combustion event subsides. Convective heating (as opposed to convective cooling) dominated the convective energy transfer event.

Fig. 2b shows a photograph taken before a controlled burn on Eglin Air Force Base in northern Florida on 1 March 2008 (identified as Eglin 1 in Table 1). The fuel bed was a 4-year-old southern rough consisting primarily of wire grass (*Aristida stricta*), long leaf pine needle cast and some turkey oak (*Quercus laevis*) leaf litter. The fuel consumed in the fire was measured at 0.38 kg m⁻². Radiative and convective heat flux data are presented in Fig. 3b. The radiation peak was found to be 75 kW m⁻² and the convection peak was 60 kW m⁻². Some

Table 1. Summary of burn environmental conditions
 Fuels are: gr, grass (various); pp, Ponderosa pine (*Pinus ponderosa*); lp, lodgepole pine (*Pinus contorta*); nc, needle cast (various); llp, long leaf pine (*Pinus palustris*); br, brush (various); sb, sagebrush (*Artemisia tridentata* subsp. *Wyomingensis*)

Name	Date	Type of fire	Fuel	Location (elevation, m)	Aspect	Slope (%)	Air temperature (K); relative humidity (%)	Wind speed (m s ⁻¹)
Rombo 1	28-Aug-2007	Surface	gr, pp nc	45°47'39.012"N, 114°8'6"W (1920)	NW	10	300; 15	0
Eglin 1	01-Mar-2008	Surface	gr, llp nc, br	30°31'39.5004"N, 86°43'41.2998"W (40)	-	0	292; 80	0.5-1
Eglin 2	02-Mar-2008	Surface	gr, llp nc	30°39'10.9002"N, 86°17'19.1004"W (65)	-	0	295; 80	0.5-1
Ichauway 1	03-Mar-2008	Surface	gr, llp nc	31°12'4.3992"N, 84°26'35.3004"W (45)	-	0	298; 50	-
Ichauway 2	05-Mar-2008	Surface	gr, llp nc	31°14'44.9988"N, 84°23'43.1982"W (50)	-	0	290; 50	0.5-1
Ichauway 3	06-Mar-2008	Surface	gr, llp nc	31°14'26.3994"N, 84°28'46.4988"W (45)	-	0	293; 58	0.5-1
Ichauway 4	06-Mar-2008	Surface	gr, llp nc	31°14'26.3994"N, 84°28'46.4988"W (45m)	-	0	293; 58	0
Rombo 2	29-Aug-2007	Brush	gr, br, pp nc	45°48'5.1834"N, 114°8'11.3634"W (1950)	S	75	302; 10	0
Leadore 1	20-May-2008	Brush	gr, sb	44°49'5.988"N, 113°17'35.6634"W (2315)	N	15	297; 15	0.5-1.5
Leadore 2	20-May-2008	Brush	gr, sb	44°49'5.988"N, 113°17'35.6634"W (2315)	N	15	297; 15	0.5-1.5
Rat Creek	16-Aug-2007	Crown	gr, lp, lp nc	45°40'44.652"N, 113°44'56.184"W (2290)	SE	20	295; 10	0
Mill Creek	30-Aug-2007	Crown	gr, lp, lp nc	46°27'52.5594"N, 113°30'34.056"W (1770)	E	5	295; 15	0

Table 2. Summary of measured fire variables
Flame angles are degrees from vertical. Rate of spread, flame length, flame depth, flame angle and residence time are based on observations from video footage of flames. Rate of spread values given in average and standard deviation in parentheses

Name	Flame spread	Time of burn	Peak radiative flux (kW m^{-2})	Peak convective flux (kW m^{-2})	Rate of spread (m s^{-1})	Flame length (m)	Flame depth (m)	Flame angle ($^{\circ}$)	Residence time (s)	Consumed fuel (kg m^{-2})
Rombo 1	Frontal	1130	20	22	0.05 (0.008)	0.83	0.68	23	42	0.47 ^A
Eglin 1	Frontal	0900	75	60	0.67 (0.40)	1.25	1.95	53	17	0.38
Eglin 2	Lateral	1100	24	13	0.18 (0.06)	0.39	0.22	28	4	0.33
Ichauway 1	Frontal	1330	115	107	0.53 (0.18)	1.59	3.12	48	12	0.57
Ichauway 2	Frontal	1020	105	100	0.17 (0.11)	0.82	0.64	20	9	0.17
Ichauway 3	Frontal	0920	90	140	0.42 (0.11)	0.84	3	33	22	0.28
Ichauway 4	Frontal	1340	59	82	0.13 (0.08)	1.25	2.33	33	11	0.38 ^A
Rombo 2	Frontal	1220	130	94	0.16 (0.03)	2.4	—	37	40	0.54 ^A
Leadore 1	Lateral	0930	120	26	0.63 (0.25)	1.44	5.2	14	10	1.67 ^A
Leadore 2	Lateral	1150	132	19	0.63 (0.25)	1.44	5.2	14	10	1.67 ^A
Rat Creek	Frontal	1320	300	42	0.8 ^B	30 ^B	40 ^B	0 ^B	—	5.25 ^A
Mill Creek	Lateral	1420	189	32	0.77 (0.39)	20	30	0	50	3.15 ^A

^AEstimated from Digital Photo Series (<http://depts.washington.edu/nwfire/dps/>, accessed 20 December 2011).

^BEstimated from daily fire growth maps and observations of fire in similar location and conditions.

of the convective peaks were quite brief and separated by time periods of zero or negative (cooling) heat flux, suggesting the passage of alternating eddies of cold and hot air, representative of environmental air and combustion products respectively. Fig. 3*b* suggests that convective heating and cooling occurred ~50 and 13% of the flaming combustion time.

A second controlled burn on Eglin Air Force Base was completed 2 March 2008 (Fig. 2*c*). This fire is designated Eglin 2 in Table 1; fuel was 1-year-old southern rough. Vegetation consumed in the flames was measured to be 0.33 kg m^{-2} . The flames approached the sensors from behind. Heat flux levels were comparatively low, with the peak radiative heat flux reaching 24 and 13 kW m^{-2} in convective heating (Fig. 3*c*). Convective heating dominated the convective energy transport.

The next set of data (identified by the label Ichauway 1 in Table 1) was collected at the Joseph W. Jones Ecological Preserve near Ichauway, Georgia. The first burn occurred 3 March 2008. The fuel bed consisted primarily of mixed grasses and longleaf pine needle cast (Fig. 2*d*). Fuel consumption was measured at 0.57 kg m^{-2} . The data exhibit radiative and convective heat flux peaks at nearly the same level, 115 and 107 kW m^{-2} (Fig. 3*d*). It appears that convective heating dominates (prevailing over 70% of the time) whereas convective cooling occurs only 5% of the time during flaming combustion.

A second Ichauway dataset (designated Ichauway 2 in Table 1) was collected 5 March 2008 (Fig. 2*e*). The fuel bed was a 1-year-old southern rough, which consisted primarily of grass and longleaf pine needle cast. Fuel consumption was measured at 0.17 kg m^{-2} . This fire spread vigorously as evidenced by the relatively high radiative and convective heat flux peak values of 105 and 100 kW m^{-2} (Fig. 3*e*). Convective heating occurred more than 50% of the flaming combustion time and cooling 25% of the time.

A third Ichauway dataset was collected 6 March, 2008 in 2-year-old southern rough (designated Ichauway 3 in Table 1). Fuels were similar to that of Ichauway 1 burn (Fig. 2*d*) but with additional brush (Fig. 2*f*). Fuel consumed in the fire was measured at 0.28 kg m^{-2} . The convective peak heat flux of 140 kW m^{-2} was far greater than the radiative heat flux peak of 90 kW m^{-2} (Fig. 3*f*). The heating and cooling fraction reveal behaviour not unlike that observed in Fig. 3*e*. Convective heating or cooling occurred 60 and 25% of the flaming combustion time.

Fig. 3*g* shows heat flux data collected in fuels similar to that shown in Fig. 2*f* (this dataset is designated Ichauway 4 in Table 1). Fuel consumed in the fire was estimated from the Digital Photo Series LLP 02 (Ottmar and Vihnanek 2000) to be 0.38 kg m^{-2} , but comparison with direct measurements on previous sites indicates that this value is likely high by 25%. Once again, convective peaks were very brief and distinct. The peak heat convective flux was 82 kW m^{-2} and radiative was 59 kW m^{-2} (Fig. 3*g*). Convective heating occurred 50% and cooling 15% of the flaming combustion time.

Brush fires

Fig. 3*h* presents heat flux data collected on the Rombo Mountain Fire 29 August 2007 (designated Rombo 2 in Table 1). This site was characterised by the presence of brush, a reasonably deep

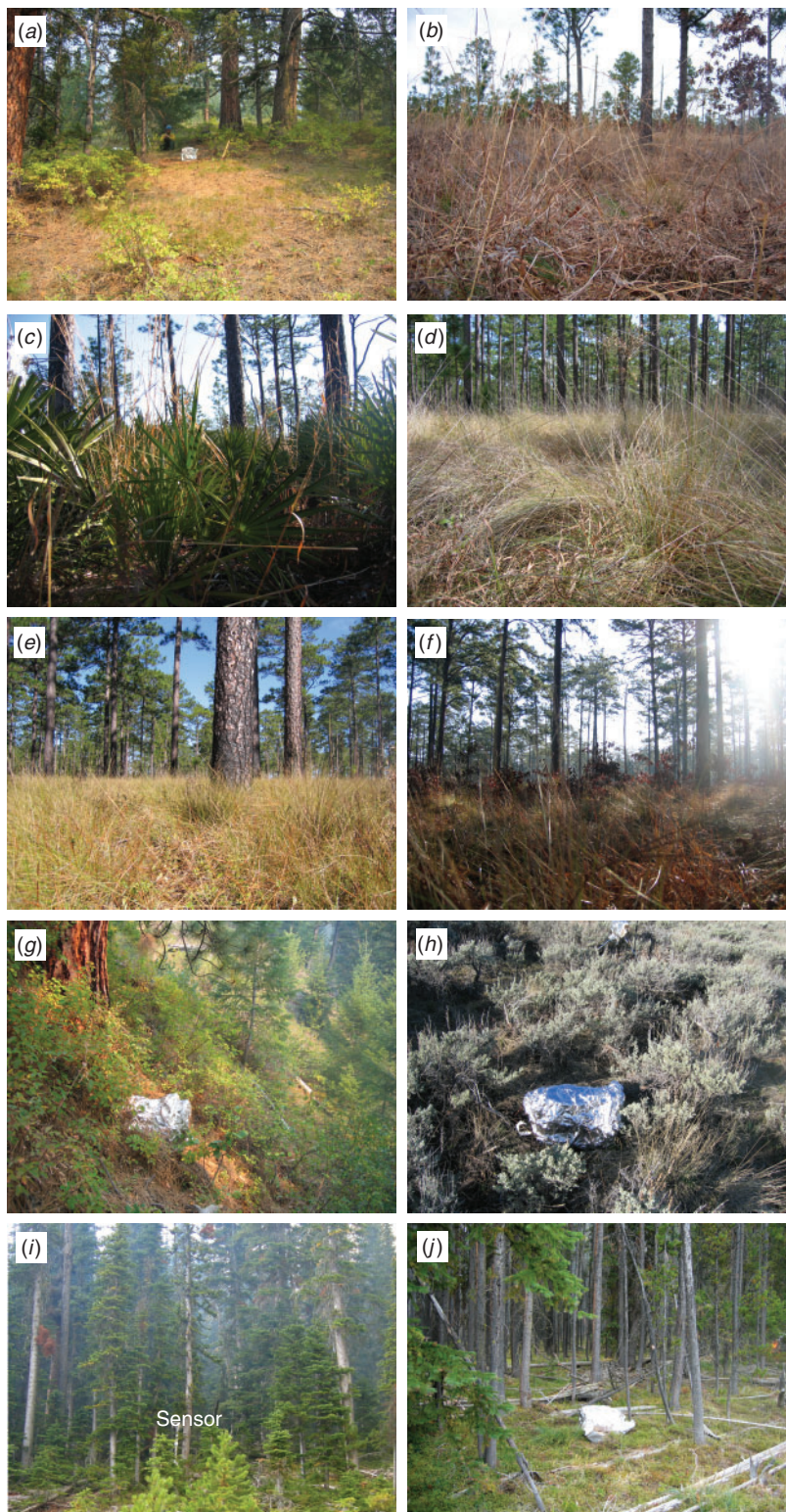


Fig. 2. Images of vegetation at sample sites taken before the fire. (a) Rombo 1 site, (b) Eglin 2 site, (c) Ichauway 2 site, (d) Eglin 1 site, (e) Ichauway 1 site, (f) Ichauway 3 and 4 site, (g) Rombo 2 site, (h) Leadore site, (i) Rat Creek site, (j) Mill Creek site.

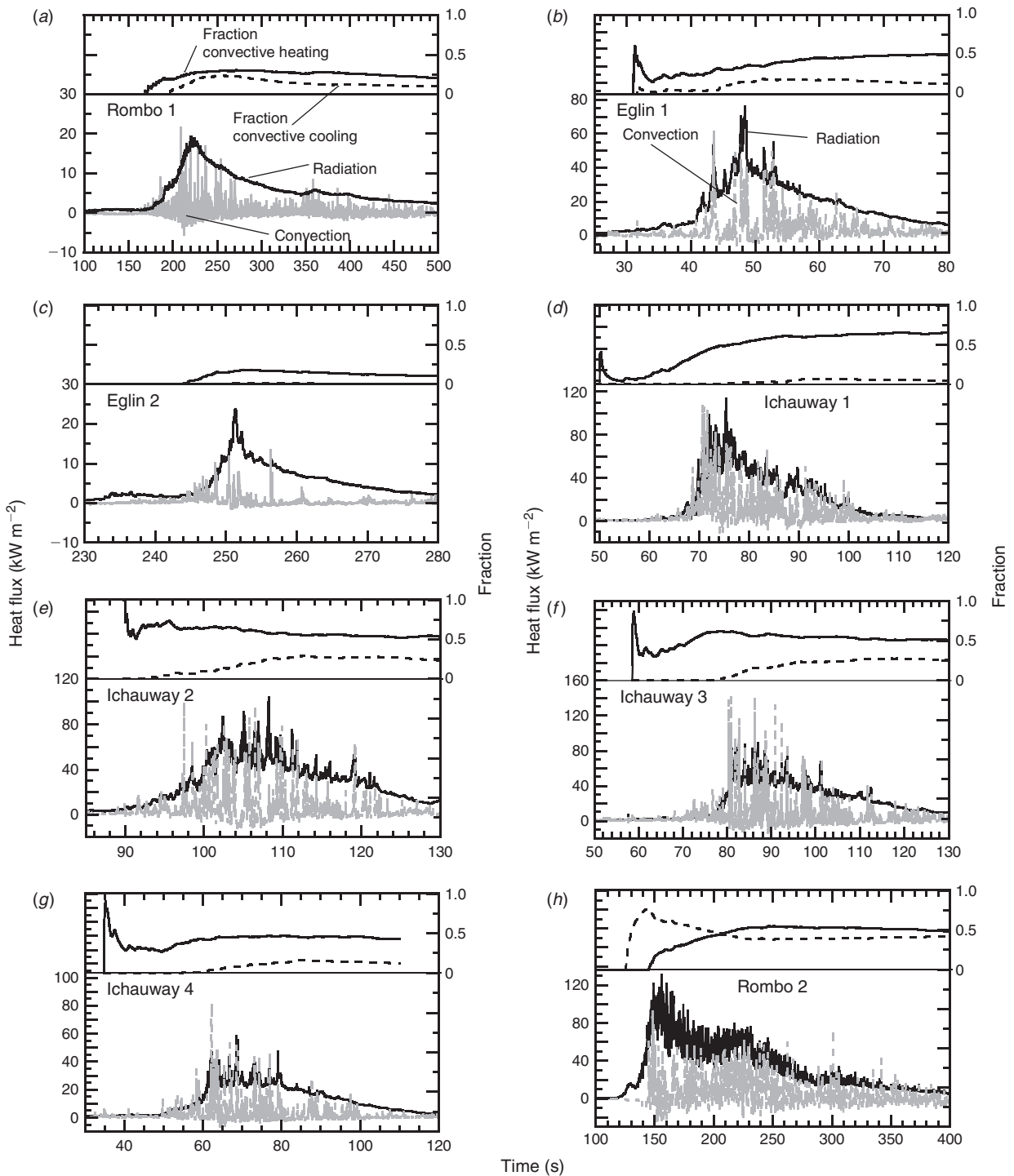


Fig. 3. Heat flux measurements for burns through Rombo 2 for: (a) Rombo 1 data; (b) Eglin 1 data; (c) Eglin 2 data; (d) Ichauway 1 data; (e) Ichauway 2 data; (f) Ichauway 3 data; (g) Ichauway 4 data and (h) Rombo 2 data. The lower or primary chart in each subplot is the convective (gray line) and radiative (black line) heat flux measurements. The upper chart in each subplot is the fraction of time that the sensor shows convective heating (solid line) or cooling (dashed line). Horizontal and vertical axes are scaled to best illustrate the heating magnitude and transient response during the flaming phase.

bed of ponderosa pine needle cast and a steep slope (Fig. 2g). Fuel consumed in the flaming combustion was estimated from the digital photo series PPJ 07 (Ottmar *et al.* 2007) to be 0.54 kg m^{-2} . Radiative heating was detected from the oncoming

flames 30 s before the flames arrived at the sensors. The upper panel of Fig. 3h shows the fraction of time the convective flux was above 1 and below -1 kW m^{-2} (respectively fraction heating and fraction cooling). It appears that while measurable

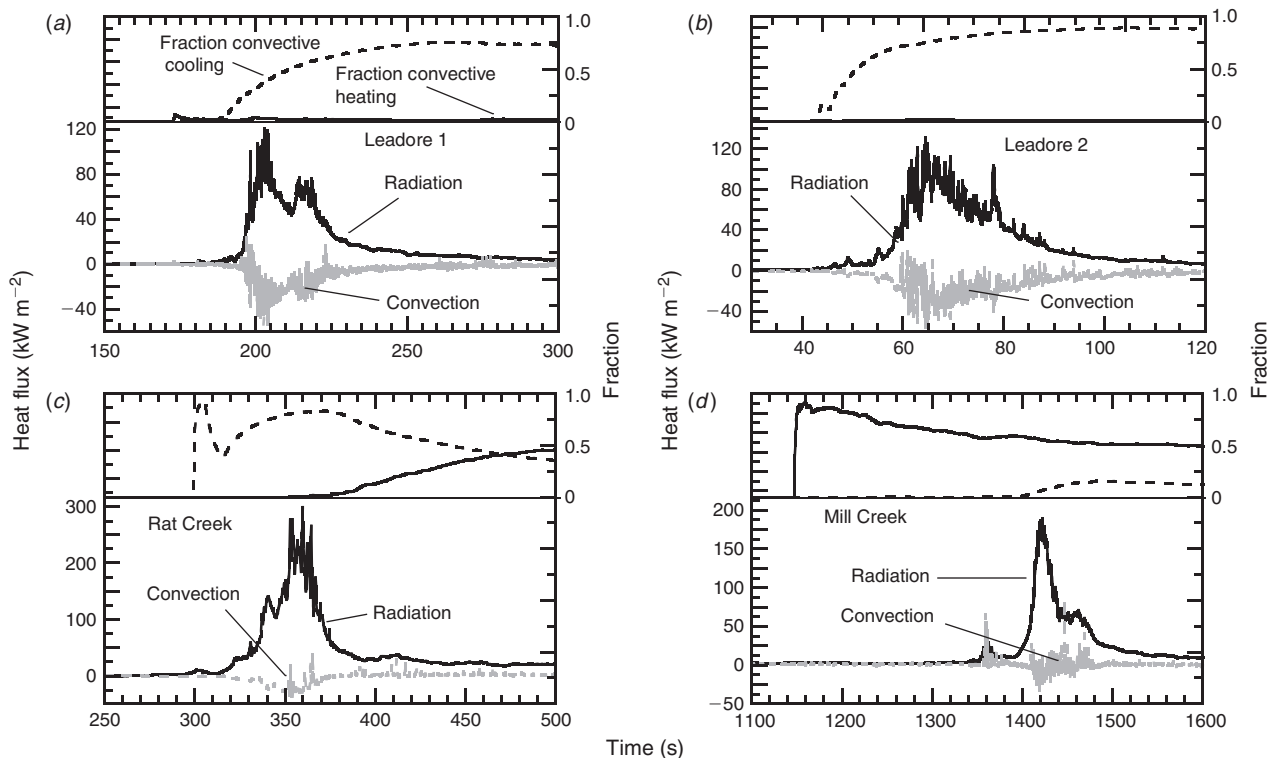


Fig. 4. Heat flux measurements for Leadore through Mill creek burns for: (a, b) Leadore 1 and 2 data; (c) Rat Creek data and (d) Mill creek data. The lower or primary chart in each subplot is the convective and radiative heat flux measurements (radiative is indicated by black solid line, convective by gray dashed line). The upper chart in each subplot is the fraction of time that the sensor shows convective heating (solid line) or cooling (dashed line). Horizontal and vertical axes are scaled to best illustrate the heating magnitude and transient response during the flaming phase.

radiative heating was occurring convective cooling dominated the convective energy transport before ignition. Apparently the air that was drawn downslope into the flames convectively cooled the sensors as they were heated by the thermal radiation emitted from the approaching flame. The flame arrival was indicated by a sharp rise in convective heating at ~ 145 s. The convective heat flux exhibited a peak of 94 kW m^{-2} , with maximum cooling of -25 kW m^{-2} . The radiative heat flux peaked at 130 kW m^{-2} and fluctuated between 40 and 130 kW m^{-2} during flaming combustion. Immediately following the commencement of the combustion event the amount of convective cooling dropped to nominally 50% as the flames arrived and convective heating increased to $\sim 60\%$.

Two sets of heat flux data collected on a prescribed burn conducted 20 May 2008 (Fig. 2h) are labelled Leadore 1 and 2 in Table 1. The fuel type was sagebrush (*Artemisia tridentata* subsp. *wyomingensis*) and mixed grasses typical of fuel type SG 10 (Ottmar *et al.* 2007). Fuel consumed in the flames was estimated at 1.67 kg m^{-2} . There was a breeze present that shifted directions throughout the burn. The fire approached the sensors laterally during the collection of both datasets. The two datasets are similar, characterised by significant radiative heating combined with primarily convective cooling (Fig. 4a, b). In fact the convective heating in this fire was so low that the fraction of time during which convective heating occurred is practically imperceptible in the graph. This is also indicated in the low observed peak convective heat flux values of

26 and 19 kW m^{-2} for the Leadore 1 and 2 burns. The peak radiative heating for the two burns was 120 and 132 kW m^{-2} .

Crown fires

Fig. 2i (top) shows the sensor location on the Rat Creek Fire 16 August 2007 in mature lodgepole pine (*Pinus contorta*). Fire conditions and data are identified by the label Rat Creek in Table 1. Fuels most closely are approximated by Digital Fuel Series LP 05 (Ottmar *et al.* 2000). Total vegetation consumed in the fire was estimated to be 5.25 kg m^{-2} . For safety reasons, no time was taken in this experiment to deploy a camera. It is known from visual observations of the fire, however, that the fire burned as a crown fire and appeared from post fire inspection to have approached the sensor as a heading fire. The sensors were positioned 1.0 m above the ground. The maximum measured radiant heat flux was nearly 300 kW m^{-2} (Fig. 4c). By contrast, peak convective heat transfer appears to be relatively low (42 kW m^{-2}). Significant convective cooling occurs in this dataset, suggesting that cool air from below the canopy was drawn past the sensors near the ground upward towards the crown fire. In either case, these radiative flux data exhibit a peak magnitude on the same order as the data of Butler *et al.* (2004), which were also collected in crown fires using a different type of sensor. This magnitude of radiative flux is reflective of radiometric flame temperatures exceeding 1500 K as gauged by the blackbody temperature corresponding to flames at this exitance.

Convective and radiative heat fluxes were recorded 30 August 2007 in a crown fire (identified as Mill Creek in Table 1). The sensors were placed in an area with a slope of 10% and little or no wind (Fig. 2j). The fuel consisted of mixed bunch grasses nominally 25 cm tall and lodgepole pine needle cast and tree crowns. Digital Photo Series type LP 05 (Ottmar *et al.* 2007) was selected as the best match for this site. Fuel loading was estimated at 5.25 kg m^{-2} but consumption was reduced to 3.15 kg m^{-2} by deducting the canopy fuel load from the estimate because the canopy did not burn completely. The fire could be best characterised as a passive crown fire. In-fire video confirmed that the fire approached the sensors laterally instead of towards the front. Although not shown here, the data and video record showed that both a surface fire event (at 550 s) and a subsequent crown fire event (at 1400 s) occurred at this site. Only the crown fire event is shown (Fig. 4d). The radiant heat peaked at 26 kW m^{-2} for the surface fire and 189 kW m^{-2} when the crown fire arrived at the sensors. The peak convective heat flux was 32 kW m^{-2} for the surface fire and 86 kW m^{-2} for the crown fire. Convective heating dominated the convective energy transfer, but the relative magnitudes were low compared with the Rat Creek crown fire measurements (Fig. 4c).

Discussion

The data presented here begin to provide a description of the variability in convective and radiative energy transfer rates from wildland fires as a function of fuel type, burning conditions and slope. Although not conclusive, the data suggest a dependence of peak heating levels on fire spread direction relative to the sensors. For the locations that experienced head fire spread (i.e. fire spreading towards the sensors) as shown in Figs 3a, b, d–h and 4c, typically the radiative flux was characterised by a period of very low heating when the flame was far away, whereas convective heating during this period was characterised by higher frequency but relatively low magnitude fluctuations. As the fire front approached the radiative heating exhibited a gradual monotonic increase with a short duration rapid rise immediately before the point of ignition of combustible products in view of the sensor. Convective heating in this region was characterised by an increase in the magnitude of the positive (heating) pulses. At ignition, both radiative and convective heating showed nearly instantaneous heating pulses. The burning period was characterised by fluctuations in the radiative heating varying from 50 to 100% of the peak levels. The convective flux varied from cooling pulses with absolute magnitudes on the order of 25% of the radiative heating to heating pulses that in some cases significantly exceeded the radiative heating. Completion of flaming was indicated by a decay in radiative heating rates and a gradual decrease in the magnitude of the convective heating and cooling pulses.

Radiative heating was characterised by temporal fluctuations of lower amplitude and frequency than for convective heating. It is posited that this occurs because radiative heating flux incident on the sensor (irradiance) was sampled from the entire hemisphere viewed by the sensors exposed to the oncoming flame, whereas convection is a local phenomenon. Thus, local fluctuations in flame conditions affected convective energy transport at the sensor, but thermal radiation sensors sampled multiple

fluctuations simultaneously and the integrated effect led to a nominally constant heat flux. Strong convective transfer fluctuations were characteristic of all 12 datasets included in this work.

For the cases where the fire approached the sensors from the side (Figs 3c, 4a, b, d) the pattern was significantly different with respect to the convective heating at ignition and during flaming. The primary difference observed was the increased magnitude of the absolute level of the cooling pulses. This trend was visible in Fig. 4a, b where the convective heating was approximately reversed from the cases where a head fire was experienced. The magnitude of the positive convective heating was low at the time of ignition and then rapidly decayed to significant convective cooling pulses that prevailed (i.e. remained negative) through the entire process. The dramatic difference in convective heating and cooling from head fires to flanking or backing fires suggests that interpretation of point measurements within the context of whole fire heat flux may be difficult with only a few sensors. Data should be interpreted with respect to sensor placement as well as the proportion of the unit that burned with each type of fire, highlighting the value of video footage of fire as it burns around the sensors.

Fig. 4c, d exhibits ground-level measurements from crown fires. Post-fire inspection of the sensor housing and surrounding vegetation burn patterns suggest that the data presented in Fig. 4c were collected during a full-scale independent crown fire. Radiative heating in this case exceeded convective heating by a factor of six. Convective energy transport was primarily cooling with very short duration positive heating pulses. The data suggest that radiative heating plays a more significant role in crown fires than in surface or brush fires, whereas the data for the surface fires indicate that convective energy transport is primarily positive and is briefly at a level comparable to or greater than is radiative heating at and shortly after ignition. It was surprising that the Mill Creek location experienced a crown fire given that a moderately intense surface fire burned through the area minutes before the crown fire. The surface fire displayed characteristics (i.e. intensity, duration) similar to the other surface fires. However, despite the consumption of the surface debris and litter, the crown fire exhibited high intensity as characterised by irradiance values captured during the event. This instance indicates the capacity for what appear to be open forest stands to sustain continuous crowning fire in the absence of surface vegetation or litter. The longest residence times were associated with the Rombo 2 and Mill Creek fires. It would be expected that fuel load would correspond to residence time, but the data presented here are inconclusive on this point. Obviously other factors contribute, such as fuel moisture content, spatial arrangement and site-specific details such as slope and wind.

Time-averaged (1-s smoothing window) radiative heat fluxes for surface fires lie between 18 and 77 kW m^{-2} , brush fires between 97 and 110 kW m^{-2} and crown fires between 179 and 263 kW m^{-2} . Fire Radiative Energy (FRE) and Fire Convective Energy (FCE) were calculated by integrating the measured convective and radiative heat fluxes and grouping the values by fire type (i.e. surface, brush and crown) (Fig. 5). The data indicate that total energy release for both modes of energy transport are closely tied to fuel type and fire intensity. The FRE data segregate by fire type,

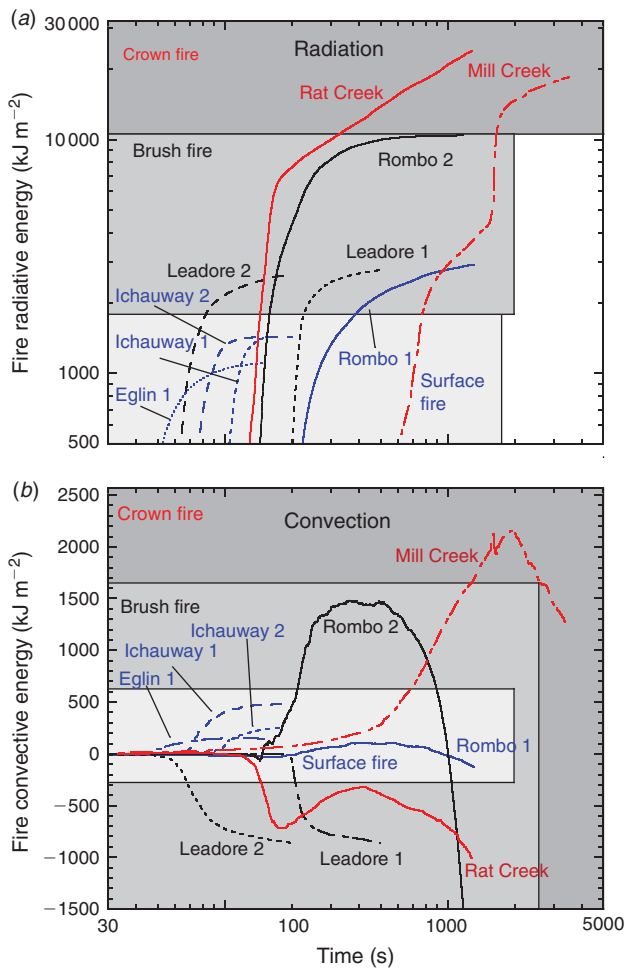


Fig. 5. Calculated fire radiative (a) and convective (b) energy as a function of fire type. The axes were modified to more clearly show the relation between fire type and energy release.

suggesting that there is link between energy release and fuel consumption. This supports work by (Kaufman *et al.* 1996) and (Wooster *et al.* 2005) that links fuel consumed to the temporal integral of the measured radiative power. The FCE data do not correlate as well with fire type. In general FCE data were roughly one order of magnitude lower than FRE. The crown fire data exhibit the greatest magnitude in FCE, but show wide fluctuation between positive and negative FCE. The brush fire data exhibit the next greatest magnitude in positive and negative FCE. The surface fire data show primarily positive FCE with negligible negative or cooling FCE. The lower correlation with fire or fuel type for the FCE data is likely due to convective heating being a local energy transfer phenomenon, whereas the FRE is a spatial phenomenon.

FRE was compared with fuel consumption for 9 of the 13 burns (Fig. 6). Clearly there is a correlation between measured FRE and fuel consumed in the fire event. The correlation presented by (Wooster *et al.* 2005; Freeborn *et al.* 2008) is also shown. The slopes of the two correlations are different, Wooster's data were collected from nadir view sensors whereas the data presented herein are from side view oriented sensors.

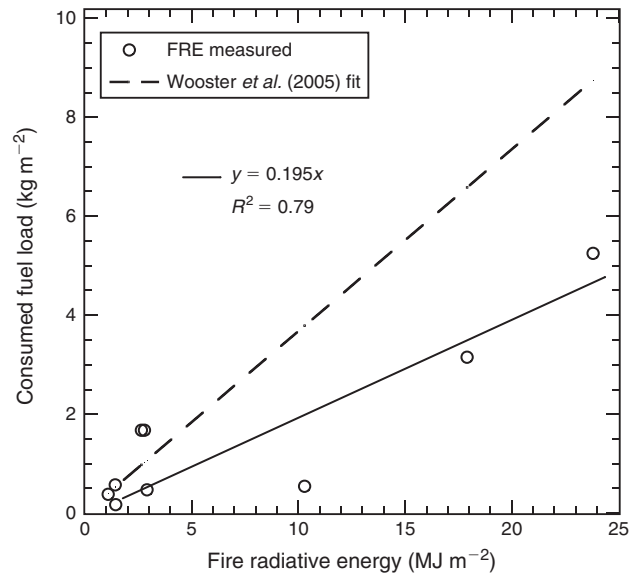


Fig. 6. Fire radiative energy (FRE) v. consumed fuel load for 9 of the 13 burns that were instrumented. The fit presented by Wooster *et al.* (2005) is also shown.

These data suggest that additional characterisation of energy release as a function of azimuthal viewing angle of wildland flames is needed.

Others have attempted to characterise convective heating from laboratory burns (Anderson *et al.* 2010). They identified several regimes: a preheating zone dominated by radiative energy transport, a convective cooling zone immediately before arrival of the flame front, and a strong convective heating zone occurring at the instant of flame front arrival and ignition. The surface fire data reported here do not fully support the laboratory model in that they show primarily convective heating immediately before ignition, followed by a rapid increase in convective heating and cooling at and subsequent to ignition. However, brush and crown fire fuel types seem to agree more closely with the laboratory-based model. In all three brush and one of the two crown fires convective energy transport was dominated by cooling before, during and after ignition. Clearly, additional investigation is needed to better characterise the role of convective energy transport in wildland fires.

Conclusions

The limited number of measurements and dependence of fire behaviour on uncontrolled environmental variables such as time of day, temperature, relative humidity, consumed fuel loading, fuel type, terrain slope and aspect, wind and fuel geometry and arrangement preclude statistically confident comparisons among datasets. One can posit fuel and environmental conditions where convective heating might play a more significant role (i.e. fine fuels and high winds) or where radiative heating would play a greater role (i.e. high fuel loading and low winds). This study presents measurements from both extremes in an effort to determine if near-ground convective energy transport varied with fuel and environment relative to radiative heat flux and if integrated convective energy and radiative energy values

correlated with fuel consumption. Radiative heat fluxes peak between 20 and 300 kW m⁻². The convective heat flux is characterised by rapid fluctuation between positive and negative convective values owing to alternating packets of cool air intermingled with hot combustion products. The convective heat flux peaks between 22 and 140 kW m⁻² (under ideal flame spread conditions). Integrated energy release correlated well with fire type for fire radiative energy, but not as clearly for fire convective energy. This work adds to the limited body of heat flux measurements in wildland fires.

Lessons learned in this effort include the importance of documenting fuel loading, fuel consumption, fuel moisture and environmental conditions before and at the time of ignition. Video images of the fire as it approaches and burns over the sensors are also critical to interpretation of results. Fuel load sampling is a labour-intensive task with significant associated analysis. This study reports direct measurements when available, but otherwise used other sources to estimate fuel consumption. Wind plays a primary role in fire behaviour, and spatial or temporal wind measurements were not collected as part of this study other than observations at the time of ignition. More intensive wind sampling should be attempted for future burns. Additional measurements are needed across all fuel and environmental types. Simplification of fuel structure such as burns in agriculture fields might be a viable option for completing repeated burns under reasonably uniform fuel conditions. Data from these studies can be obtained by contacting the corresponding author.

Acknowledgements

This work was only accomplished through the cooperation of many Fire Managers and Fire Incident Management Teams. We are especially grateful to George Johnson of the BLM for his willingness to accommodate our research efforts in his prescribed burns. We also acknowledge the financial support for at least part of this effort from the Joint Fire Science Program, the Fire, Fuels, and Smoke Program of the US Forest Service Missoula Fire Sciences Laboratory, and the National Fire Plan.

References

- Albini FA (1996) Iterative solution of the radiation transport equations governing spread of fire in wildland fuel. *Combustion, Explosion, and Shock Waves* **32**, 534–543. doi:10.1007/BF01998575
- Anderson, HE (1969) Heat transfer and fire spread. USDA Forest Service, Intermountain Forest and Range Experiment Station, Research Paper INT 69, pp. 1–20. (Ogden, UT)
- Anderson WR, Catchpole EA, Butler BW (2010) Convective heat transfer in fire spread through fine fuel beds. *International Journal of Wildland Fire* **19**, 284–298. doi:10.1071/WF09021
- Butler BW (1993) Experimental measurements of radiant heat fluxes from simulated wildfire flames. In '12th International Conference of Fire and Forest Meteorology, Oct. 26–28, 1993. Jekyll Island, Georgia', Oct. 26–28, 1993. (Eds JM Saveland, J Cohen) Volume 1, pp. 104–111. (Society of American Foresters: Bethesda, MD)
- Butler BW, Cohen JD (1998) Firefighter safety zones: a theoretical model based on radiative heating. *International Journal of Wildland Fire* **8**, 73–77. doi:10.1071/WF9980073
- Butler BW, Cohen J, Latham DJ, Schuette RD, Sopko P, Shannon KS, Jimenez D, Bradshaw LS (2004) Measurements of radiant emissive power and temperatures in crown fires. *Canadian Journal of Forest Research* **34**, 1577–1587. doi:10.1139/X04-060
- Cruz MG, Butler BW, Viegas DX, Palheiro P (2011) Characterization of flame radiosity in shrubland fires. *Combustion and Flame* **158**, 1970–1976. doi:10.1016/J.COMBUSTFLAME.2011.03.002
- Freeborn PH, Wooster MJ, Hao WM, Ryan CA, Nordgren BL, Baker SP, Ichoku C (2008) Relationships between energy release, fuel mass loss, and trace gas and aerosol emissions during laboratory biomass fires. *Journal of Geophysical Research* **113**, D01301. doi:10.1029/2007JD008679
- Kaufman Y, Remer L, Ottmar R, Ward D, Rong RL, Kleidman R, Fraser RH, Flynn L, McDougal D, Shelton G (1996) Relationship between remotely sensed fire intensity and rate of emission of smoke: SCAR-C experiment. In 'Global Biomass Burning'. (Ed. J Levine) pp. 685–696. (MIT Press: Cambridge MA)
- King AR (1961) Compensating radiometer. *British Journal of Applied Physics* **12**, 633. doi:10.1088/0508-3443/12/11/311
- Morandini F, Silvani X, Rossi L, Santoni P-A, Simeoni A, Balbi J-H, Louis Rossi J, Marcelli T (2006) Fire spread experiment across Mediterranean shrub: influence of wind on flame front properties. *Fire Safety Journal* **41**, 229–235. doi:10.1016/J.FIRESAF.2006.01.006
- Ottmar RD, Vihnanek R (2000) Stereo photo series for quantifying natural fuels. Volume VI: longleaf pine, pocosin, and marshgrass types in the Southeast United States. National Wildfire Coordinating Group, National Interagency Fire Center, PMS 835. (Boise, ID)
- Ottmar R, Vihnanek R, Wright CS (2000) Stereo photo series for quantifying natural fuels. Volume III: lodgepole pine, quaking aspen, and gambel oak types in the Rocky Mountains. National Wildfire Coordinating Group, National Interagency Fire Center, PMS 832. (Boise, ID)
- Ottmar RD, Vihnanek R, Wright CS (2007) Stereo photo series for quantifying natural fuels. Volume X: sagebrush with grass and ponderosa pine-juniper types in central Montana. USDA Forest Service, Pacific Northwest Research Station, General Technical Report PNW-GTR-719. (Portland, OR)
- Packham D, Pompe A (1971) Radiation temperatures of forest fires. *Australian Forest Research* **5**, 1–8.
- Santoni PA, Simeoni A, Rossi JL, Bosseur F, Morandini F, Silvani X, Balbi JH, Cancellieri D, Rossi L (2006) Instrumentation of wildland fire: characterisation of a fire spreading through a Mediterranean shrub. *Fire Safety Journal* **41**, 171–184. doi:10.1016/J.FIRESAF.2005.11.010
- Silvani X, Morandini F (2009) Fire spread experiments in the field: temperature and heat fluxes measurements. *Fire Safety Journal* **44**, 279–285. doi:10.1016/J.FIRESAF.2008.06.004
- Wooster MJ, Roberts G, Perry GLW, Kaufman YJ (2005) Retrieval of biomass combustion rates and totals from fire radiative power observations: FRP derivation and calibration relationships between biomass consumption and fire radiative energy release. *Journal of Geophysical Research* **110**, D24311. doi:10.1029/2005JD006318
- Yedinak KM, Forthofer JM, Cohen JD, Finney MA (2006) Analysis of the profile of an open flame from a vertical fuel source. *Forest Ecology and Management* **234**(Suppl.), S89. doi:10.1016/J.FORECO.2006.08.125